Kinetics of particle deposition at heterogeneous surfaces

D.Lj. Stojiljković, S.B. Vrhovac *

Scientific Computing Laboratory, Center for the Study of Complex Systems, Institute of Physics Belgrade, University of Belgrade, Pregrevica 118, Zemun 11080, Belgrade, Serbia

H I G H L I G H T S

- Kinetics of spherical particle deposition on a patterned substrates is studied.
- Patterns consist of square cells centered at the vertices of a square lattice.
- Cell size α and cell–cell separation β have a striking influence on the kinetics.
- When $\beta + \alpha/2 < 1$, asymptotic approach of the coverage to the jamming limit is algebraic.
- Spatial distribution of particles inside the cell at the jammed state is studied.

A R T I C L E   I N F O

A B S T R A C T

The random sequential adsorption (RSA) approach is used to analyze adsorption of spherical particles of fixed diameter d_0 on nonuniform surfaces covered by square cells arranged in a square lattice pattern. To characterize such pattern two dimensionless parameters are used: the cell size α and the cell–cell separation β, measured in terms of the particle diameter d_0. Adsorption is assumed to occur if the particle (projected) center lies within a cell area. We focus on the kinetics of deposition process in the case when no more than a single disk can be placed onto any square cell ($\alpha < 1/\sqrt{2} \approx 0.707$). We find that the asymptotic approach of the coverage fraction $\theta(t)$ to the jamming limit θ_J is algebraic if the parameters α and β satisfy the simple condition, $\beta + \alpha/2 < 1$. If this condition is not satisfied, the late time kinetics of deposition process is not consistent with the power law behavior. However, if the geometry of the pattern approaches towards "noninteracting conditions" ($\beta > 1$), when adsorption on each cell can be decoupled, approach of the coverage fraction $\theta(t)$ to θ_J becomes closer to the exponential law. Consequently, changing the pattern parameters in the present model allows to interpolate the deposition kinetics between the continuum limit and the lattice-like behavior. Structural properties of the jammed-state coverings are studied in terms of the radial distribution function $g(r)$ and spatial distribution of particles inside the cell. Various, non-trivial spatial distributions are observed depending on the geometry of the pattern.

© 2017 Elsevier B.V. All rights reserved.

1. Introduction

The adsorption of particles on a flat substrate is a common phenomenon which has a great scientific and industrial importance as it has been linked to a wide range of applications in biology [1–4], nanotechnology [5,6], device physics [7–9],

---

* Corresponding author.
E-mail addresses: danica@ipb.ac.rs (D.Lj. Stojiljković), vrhovac@ipb.ac.rs (S.B. Vrhovac).
URLs: http://www.scl.rs/danica/ (D.Lj. Stojiljković), http://www.ipb.ac.rs/~vrhovac/ (S.B. Vrhovac).

physical chemistry [10,11], and materials science [12]. Depending on the application in question, the depositing objects could be colloidal particles, polymer chains, globular proteins, nanotubes, DNA segments, or general geometrical shapes, such as disks, polygons, etc. Due to its wide range of applications, there has been continuing effort to enrich our understanding of deposition processes and experimentally observed structural properties of the adsorbed phase [13–15].

The kinetics of adsorption has been mainly studied through the formulation of different models, aiming to capture the essential features of the deposition process. Random Sequential Adsorption (RSA) is the simplest model that can still provide the generic features of the adsorption phenomenon for the case of very strong interaction between particles and the substrate (for a review on RSA models see [13]). In the RSA model, adsorption process is considered as sequential addition of particles on the substrate such that at each time step only one particle is added on the substrate at a randomly selected position. During the process of addition, newly adding particles are forbidden from overlapping with the already adsorbed particles and any attempt of adsorption resulting in an overlap is rejected. The adsorbed particles are permanently fixed at their spatial positions so that they affect the geometry of all later placements. Under these conditions, the system evolves rapidly toward nonequilibrium conditions and the kinetics becomes essentially dominated by geometrical exclusion effects between particles. The most common parameter to characterize the kinetic properties of a deposition process is the coverage $\theta(t)$, defined as the fraction of the substrate area covered by the adsorbed particles at time t. Due to the blocking of the substrate area by the already randomly adsorbed particles, at large times the coverage $\theta(t)$ approaches the jammed-state value θ_J, where only gaps too small to fit new particles are left in the monolayer.

Although RSA model formulated under those conditions may accurately reproduce many experimental situations, its extension to more complex surfaces having an intrinsic structure is by no means trivial. For example, the supporting surface may be prepatterned with preferential sites for specific particle attachment, which may alter the kinetics of the process and the structure of the adsorbed layer. With the use of photolithographic techniques, high-power lasers, chemical treatments, etc., such surface modifications are routinely realized on the microscale, or even on the nanoscale [16–19].

It must be stressed that the classical RSA approach can be used for modeling the kinetics of an idealized process only, consisting in the creation of particles at a given distance from the interface with a constant rate and in a consecutive manner. For particles of a submicrometer size range, in addition to hydrodynamic and electrostatic forces, Brownian motion significantly affects their trajectories and transport to boundary surfaces. It is not possible, within the framework of the RSA model, to find a unique relationship between the kinetics of this idealized process and the kinetics of the particle adsorption process governed by various transport mechanisms. One has, therefore, to rely on approximate models being useful for specific transport mechanisms of particles [20].

There is a well-developed literature on irreversible adsorption on various types of two-dimensional (2D) patterned surfaces [21–29]. Specifically, pre-patterned substrates have been studied in a model of irreversible deposition on a random site surface (RSS), where the sites are represented by randomly distributed points [21,23]. Adamczyk et al. [24] have extended the RSS model to the situation where the size of the landing sites, in the shape of circular disks, is finite and comparable with the size of adsorbing spheres. Araújo et al. [28] and Marques et al. [29] have investigated the adsorption of disk-shaped particles on a patterned substrate consisted of equal square cells centered at the vertices of a square lattice. They studied the effect of the presence of a regular substrate pattern and particle polydispersity on the deposit morphology and density, as well as on the in-cell particle population. In addition, Araújo [30] has discussed the influence of the pattern on the adsorption kinetics. He has pointed out that time evolution towards the jammed state can be consistent with exponential or power-law behavior, depending on the geometry of the pattern.

Recently, motivated by nano-patterning, we have analyzed irreversible deposition of spherical particles of a fixed radius on nonuniform flat surfaces covered by non-overlapping rectangular cells that are *randomly* placed and fixed on the substrate surface [31]. The basic assumption of our model is that a particle can only be adsorbed if the center of its disk-shaped projection lies within one of the landing cells. We have studied structural properties of the jammed-state coverings in terms of the radial distribution function $g(r)$ and distribution of the Delaunay 'free' volumes $P(v)$. Pore distribution $P(v)$ has been widely used to characterize the organization of grains at the local level in disordered granular packings and to quantify the structural changes of the packing during the compaction process [32–36]. The convenient definition of a pore is based on the Delaunay triangulation. Delaunay decomposition is a natural way to subdivide a planar structure of disks into a system of minimal triangles with vertices on the centers of neighboring disks chosen in such a way that no other disks in the structure have centers within the circumcircle of each Delaunay triangle. One of the advantages of such decomposition is that it does not require the introduction of any threshold. Pore (Delaunay "free" volume) is defined as a part of the Delaunay triangle not occupied by the disks [34,35]. It was shown that the porosity (pore volumes) of deposited monolayer can be controlled by the size and shape of landing cells, and by anisotropy of the cell deposition procedure [31]. Furthermore, we have shown that in the case of low densities of landing cells $\theta_0^{(cell)} \approx 0.1$ the plot of the first derivative of coverage fraction $\theta(t)$ with respect to time t at the very late times of the deposition process is not linear on a double logarithmic scale, indicating that the approach to the jamming limit is not consistent with the power law behavior given by the time dependence:

$$\theta_J - \theta(t) \sim t^{-1/d}. \tag{1}$$

For irreversible deposition of spherically symmetric particles on continuum substrate, the above relation (1) was numerically and analytically confirmed valid by many investigators [3,37–40]. Parameter d is interpreted as substrate dimension [37] in the case of spherical particles adsorption or, more generally, as a number of degrees of freedom [41]. In addition, our results have suggested that in the case of single particle per-cell adsorption and low densities of landing cells the approach to the

jamming limit can be exponential, as in lattice RSA models [42–45]. For discrete substrates the approach of the coverage fraction $\theta(t)$ to its jamming limit θ_J is given by the time dependence:

$$\theta_J - \theta(t) \sim \exp(-t/\sigma), \tag{2}$$

where parameter σ depends on the orientational freedom of depositing objects, and on the dimensionality of the substrate [44,45].

The difference between deposition on finite-size landing cells and lattice RSA is in the particle positions, which can be uncertain within the order of the size of the cell in the former case. Very recently Privman and Yan [46] have analyzed both numerically and analytically extended model of one-dimensional deposition of segments of length a, on a lattice of spacing ℓ between its sites, which instead of just being lattice points are symmetrically broadened (about the lattice points) into segments of width w in which the centers of the depositing objects can land. They reported that even an arbitrarily small imprecision in the lattice-site localization ($w \gtrsim 0$) changes the convergence to jamming from fast, exponential (2), to slow, power-law (1). The present study in similar spirit investigates the rapidity of the approach to the jamming state in the case of *two-dimensional* (2D) prepatterned substrate. Unlike the models studied in our previous work [31], here we analyze deposition on the substrates patterned with a square grid of square-shaped cells onto which the particle can adhere. We consider the process of the irreversible random sequential adsorption (RSA) of fixed size disks. The present work is focused on the effect of the presence of a regular substrate pattern on the temporal evolution of the coverage fraction $\theta(t)$. Our aim is to quantify changes in time coverage behavior $\theta(t)$ at densities near jamming limit θ_J, associated with different cell size and density.

The rest of the article is organized as follows. In Section 2 we introduce the model and give some details of our simulations. We present the simulation results and discussions in Section 3. Finally, Section 4 contains some additional comments and final remarks.

2. Model and numerical simulation

We study irreversible monolayer deposition of identical disks onto a prepared flat nonuniform substrate, where the interparticle interaction is limited to hard-core exclusion. The substrate heterogeneities consist of non-overlapping (identical) square cells that are fixed on the substrate surface. The landing cells are arranged to form a regular pattern, i.e. squares are centered at the vertices of a square lattice and their edges are oriented parallel to the lattice principal axes. A disk is irreversibly adsorbed at random position on the substrate if it does not overlap any of previously adsorbed particles and if the center of disk lies inside one of the cells. Adsorbed disks are permanently fixed to their spatial positions.

The geometry of the pattern is controlled by the two dimensionless parameters, α and β, measured in terms of the particle diameter $d_0 = 2r_0$. Parameter α is the cell size, and parameter β is the shortest distance between the parallel sides of the nearest neighboring cells. The Monte-Carlo simulations are performed on a planar substrate with typically 256×256 landing cells. In order to estimate coverages with higher precision, the number of cells is increased to 1024×1024 for some landing-cell configurations (their specifications are provided later in the text). Periodic boundary conditions are used in all directions.

In numerical calculations, the time t is gradually increased by an increment Δt, given by $\Delta t = \pi r_0^2/L^2$, each time an attempt is made to deposit a disk of radius $r_0 = d_0/2$ on a square surface (collector) of area L^2. Consequently, we define dimensionless adsorption time $t = N_{att}\pi r_0^2/L^2$, where N_{att} is the overall number of attempts to place disk particles. By plotting coverage $\theta(t)$ versus the adsorption time t, defined above, one can simulate the kinetics of particle adsorption. However, in order to optimize the computing time, deposition is attempted only inside the cells. We chose a random cell and attempt to deposit a particle at random position within that cell. This optimization affects time scaling, so that the time increment can be calculated as $\Delta t = \frac{\pi r_0^2}{L^2}\frac{(\alpha+\beta)^2}{\alpha^2}$. In some cases, we wanted to reach very large times which required further optimizations of our calculations. When cells are small enough and can be occupied by one particle at most, we try to achieve the deposition events only at free cells. Then, the time t is increased after every deposition attempt by an increment $\Delta t = \frac{\pi r_0^2}{N_{free}}\frac{(\alpha+\beta)^2}{\alpha^2}$, where N_{free} is the number of free cells.

Depending on the cell size α, one can place one or more disk centers inside each cell. For $\alpha < 1/\sqrt{2} \approx 0.707$, at most a single disk can be adsorbed at any given square cell. We denote this case as single particle per-cell adsorption (SPCA). For squares with $\alpha \geq 1/\sqrt{2}$, more than a single disk can be placed in the square cell, and we denote this as multiparticle per-cell adsorption (MPCA). For distances between neighboring cells $\beta < 1$, a disk attempting adsorption on a given cell can overlap with a previously adsorbed one belonging to a neighboring cell, resulting in a failed adsorption attempt. This excluded volume "interaction" between particles during adsorption at *different* cells affects the overall structure of the adsorbed layer and causes slower asymptotic approach of the coverage fraction $\theta(t)$ to its jamming limit [28,31]. Such regime is denoted *interacting cell–cell adsorption* (ICCA). For $\beta \geq 1$, disks attempting adsorption cannot overlap other disks in neighboring cells, yielding the *noninteracting cell–cell adsorption* regime (NICCA). Deposition kinetics in the regime of NICCA is completely determined by the kinetics of adsorption of particles on finite size substrate (a single cell) with appropriate boundary conditions [28,31].
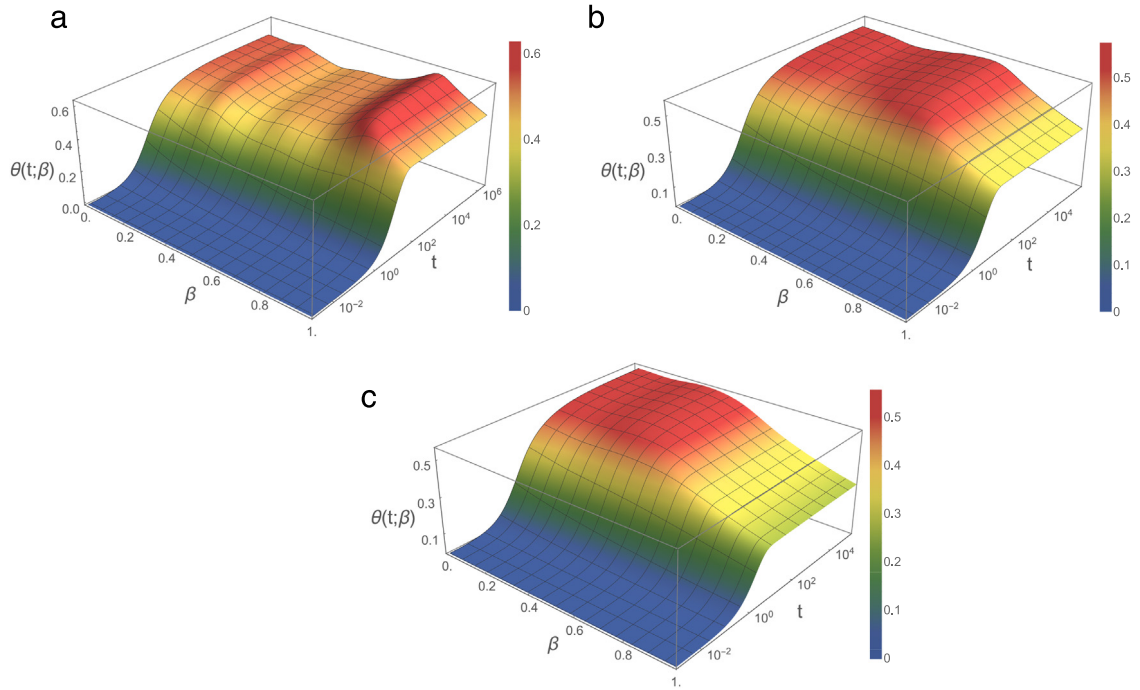
Fig. 1. Shown here is dependence of the time evolution of the coverage fraction $\theta(t)$ on the gap size β between landing cells (in units of the disk diameter d_0), for the three values of cell size, $\alpha = 0.3$ (a), 0.5 (b), and 0.7 (c). For each α, the gap β between cells is varied in the range [0, 1], with the step of 0.02.

3. Results and discussion

3.1. Effect of varying β on the long-time adsorption kinetics

In this work we focus on the interacting cell–cell adsorption (ICCA) regime in the case of single particle per-cell adsorption (SPCA). Kinetics of the irreversible deposition of disks is illustrated in Fig. 1(a)–(c) where the plots of time coverage behavior $\theta(t)$ are given for the three values of cell size, $\alpha = 0.3, \ 0.5,$ and 0.7. Here, the plots of such time-dependence are shown for various values of the gap β between the cells, in the range from $\beta = 0$ (continuous substrate and ICCA regime) to $\beta = 1$ (upper limit of the parameter β, above which the NICCA occurs). These 2D plots enable us to analyze how the time evolution of the coverage $\theta(t)$ in the case of SPCA depends on the gap size β between the landing cells. It can be seen that for a fixed size of landing cells α, coverage $\theta(t)$ in the early stage of the deposition process increases faster when the gaps between the cells are smaller. Indeed, at very early times of the process, when the coverage fraction $\theta(t)$ is small, deposited object do not "feel" the presence of the other ones, and the coverage grows rapidly in time. Then, adsorption process has overall rate proportional to the surface density of landing cells onto which the particles can adhere. Since the flux of incoming particles is fixed, the overall rate at which the coverage $\theta(t)$ increases is progressively reduced with increasing of the gap between the landing cells.

At late enough time, when the coverage fraction is sufficiently high to make "excluded volumes" for deposited objects begin to overlap, there is a strong dependence of the adsorption rate on the parameter β. Reduction of the rate of adsorption events that occurs, with decreasing of the gap size β, corresponds to increasing of the impact the cell–cell excluded volume interaction on the late stage of the deposition process.

It is interesting to emphasize that the dependence of the jamming coverage θ_J is a nonmonotonic function of the gap size β (see Fig. 1). It goes from jamming coverage for continuum $\theta_J^{\mathrm{cont}} = 0.5472 \pm 0.0002$ [47] ($\beta = 0$), reaches some local minima ($0 < \beta < 1$), and tend to a definite value which corresponds to the coverings when each cell is occupied by a single particle. Corresponding explanations of such variations of the jamming coverage θ with parameter β are provided later in the text.

In order to gain a better insight into the complex kinetics of SPCA in the ICCA regime, it is useful to analyze in particular the temporal evolution of the first derivative of coverage $\theta(t)$ with respect to time t. The time derivatives of $\theta(t)$ are calculated numerically from the simulation data. Representative examples of double logarithmic plots of the time derivative $d\theta/dt$ are shown in Fig. 2(a)–(c), for the three values of cell size, $\alpha = 0.3$ (a), 0.5 (b), 0.7 (c). For each α, results are presented for various values of the gap β between the cells in the range $0.60 \leqslant \beta \leqslant 0.98$. In the case of the algebraic behavior of the coverage fraction $\theta(t)$ (see Eq. (1)), a double logarithmic plot of the first time derivative $d\theta/dt \propto t^{-(1+d)/d}$ is a straight line. As seen
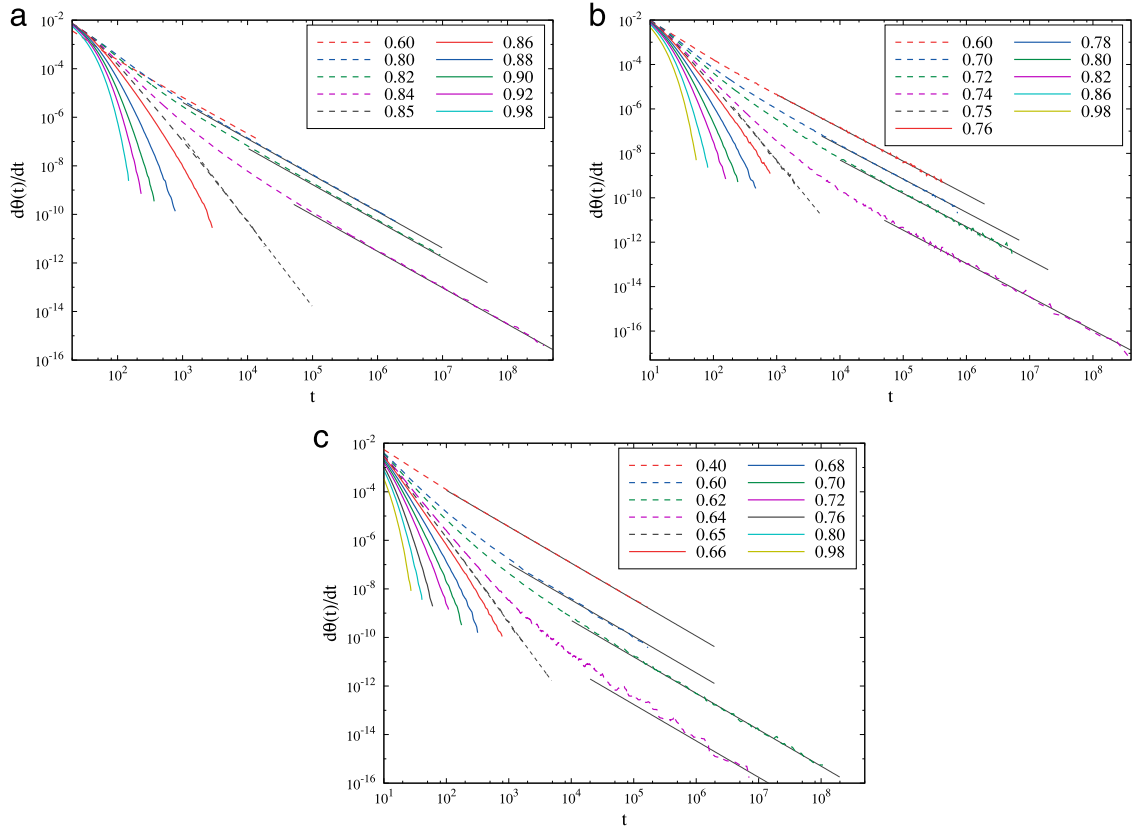
Fig. 2. Test for the presence of the algebraic law (1) in the approach of the coverage $\theta(t)$ to the jamming limit θ_J for different values of cell size, $\alpha = 0.3$ (a), 0.5 (b), and 0.7 (c). The curves in each graph correspond to various values of the gap β between the cells, as indicated in the legend. Straight line sections of the curves show where the law holds. The solid straight lines have the slope $-3/2$ and are guides for the eye. The dashed straight line has slope $-5/2$ indicating the late time RSA behavior of the system for the critical values of the parameter β: (a) $\beta_c = 0.85$, (b) 0.75, (c) 0.65 (see Eq. (4)).

from Fig. 2, if the values of parameter β for cells of size $\alpha = 0.3, \; 0.5, \; 0.7$ do not exceed, respectively, $\approx 0.84, \; 0.74$ and 0.64, the late time kinetics of deposition process is similar to the one observed for disks with equal size, adsorbing on a clean substrate. Additionally, thin straight lines with the slope $-3/2$ are shown in Fig. 2, indicating the late time RSA behavior for clean continuous substrates [3,37–40]. However, the same is not valid for large values of the parameter β, regardless of the cell size α (obviously, $\alpha < 1/\sqrt{2} \approx 0.707$ in the case of SPCA). As it can be seen, at the late times of the deposition process the plots of $d\theta/dt$ *vs. t* are not linear on a double logarithmic scale for sufficiently large values of the gap β. The deviation from the power law (1) is particularly pronounced for low densities of landing cells, i.e. when $\beta \lesssim 1$.

Theoretical arguments supporting Feder's law (1) have been presented by Swendsen [37] and Pomeau [38]. Their analysis is based on the exclusion of the area of radius d_0 around each disk of radius $d_0/2$ for selecting the center of the newly arriving disk. After a certain time, characterizing the beginning of the asymptotic regime, the area that is available to the center of a new disk consist of small disconnected areas that can be occupied by only one additional disk. When power law (1) holds, a vanishing-small area that is available for the insertion of a new particle can be created with non-zero probability during the deposition process. Arbitrarily small areas are reached with very small probability for a uniform flux of the arriving disks that attempt deposition. In the case of ICCA-SPCA, since only one particle can fit per-cell, the existence of minimum finite area is related with particles previously adsorbed on neighboring cells. As seen from Fig. 3(a), particles adsorbed on neighboring cells can completely overlap the cell when the gap β and cell size α satisfy the relation [30]:

$$\beta + \alpha/2 < 1. \tag{3}$$

Hence, below the critical value of the parameter β,

$$\beta_c = 1 - \alpha/2, \tag{4}$$

there is no minimum *finite* area available to accommodate one particle. However, above the critical value β_c particles adsorbed on neighboring cells cannot prevent adsorption inside the cell. Then, there exist finite regions where the center of a disk can land without overlapping a previously adsorbed particle (see Fig. 3(b)). For the critical value of the gap β_c approach
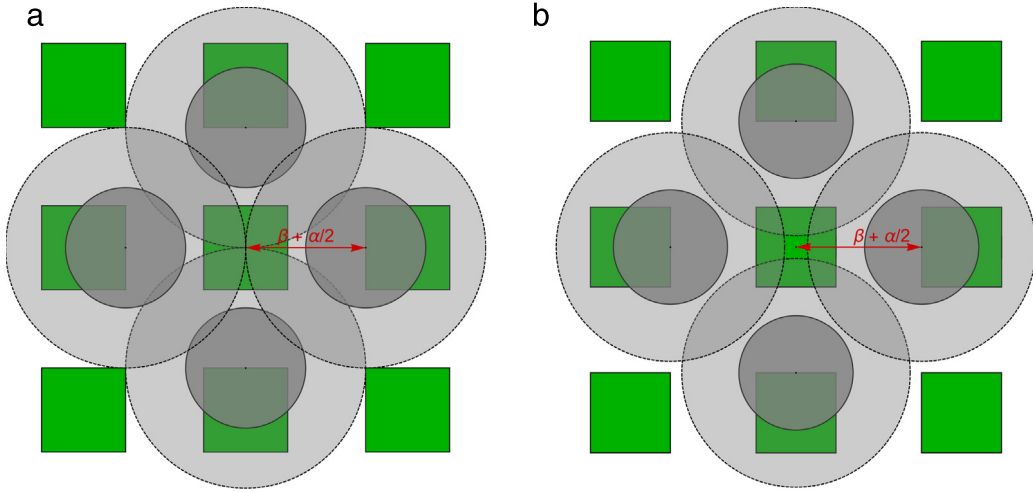
Fig. 3. Illustration of how a particles adsorbed in a neighboring cells can prevent adsorption on the central cell: (a) the overlap of the shadowed regions of the four neighboring particles completely overlap the central cell; (b) particles adsorbed on neighboring cells cannot prevent adsorption inside the cell.

to the jamming coverage θ_J with time is still algebraic (1), with the exponent that approximately equals to $-5/2$ which does not depend on the cell size α.

Our numerical results suggest that for $\beta_c < \beta < 1$, the asymptotic approach of the coverage fraction $\theta(t)$ to its jamming limit θ_J is neither algebraic nor exponential. Semilogarithmic plots of the time derivative $d\theta/dt$ are shown in Fig. 4(a)–(c), for three values of the cell size, $\alpha = 0.3$ (a), 0.5 (b), 0.7 (c). For each α, results are displayed for various values of the parameter β above the corresponding critical values (see Eq. (4)), $\beta_c = 0.85$ (a), 0.75 (b), 0.65 (c). One clearly observes that for the fixed value of cell size α, the time derivatives of $\theta(t)$ decays at the very late times of the deposition process more quickly for the larger values of the gap β between the cells. Interestingly, in the limit of $\beta \to 1$ approach of coverage $\theta(t)$ to the jamming limit θ_J is exponential of the form (2). The characteristic timescale σ is found to decrease with the cell size α according to power-law, $\sigma \propto \alpha^{-2.04\pm0.02}$. In other words, the relaxation time σ in Eq. (2) is inversely proportional to the cell area. It must be stressed that the appearance of even a slight cell–cell excluded volume interaction violates the exponential asymptotic approach (2).

### 3.2. Influence of the pattern on the jamming density θ_J

Let us go back to the analysis of the nonmonotonic behavior of the jamming density θ_J as a function of the gap size β between the landing cells observed in Fig. 1. Dependences of the jamming coverage θ_J on the separation distance $\alpha + \beta$ between cell centers are presented in Fig. 5 for the three values of cell size, $\alpha = 0.3$, 0.5 and 0.7. For the case of SPCA, jamming coverage θ_J can be exactly calculated for β larger than the critical value β_c (Eq. (4)) [28]. Indeed, since each cell at late enough time contains the center of a single deposited particle, the jamming coverage is simply

$$\theta_J^c = \frac{r_0^2 \pi}{(\alpha + \beta)^2}. \tag{5}$$

The solid black line in Fig. 5 indicates values of the jamming coverages calculated from Eq. (5). The jammed-state value $\theta_J^{cont} = 0.5472 \pm 0.0002$ [47] of the coverage in the case of the irreversible disks deposition on continuum substrate is marked on the same figure by horizontal dashed line. When gap between the cells β starts to increase, cell–cell excluded volume interaction is still strong, but substrate area that is available for the insertion of a new particle is reduced, which leads to decrease of the jamming coverage below the value for continuum θ_J^{cont}. As a gap size β increases further, the cell–cell excluded volume interaction weakens, but one expects a higher impact of patterning of the surface on the local particle arrangements. An increase in the pattern-induced tendency for semiordering of the coverings leads to the formation of jammed-state deposits of higher density. Then, for sufficiently large values of parameter β, jamming coverage exceeds the jamming limit θ_J^{cont} for continuum substrate and continues to grow with β. In this case, the theoretical value of the highest possible coverage fraction is equal to $\pi/4 \approx 0.7854$. This value corresponds to the local configurations of quadratic symmetry when the disk centers are located at the vertices of a square with a side of $\alpha + \beta = 1$ [48]. However, in the present model this maximum of the jamming coverage θ_J is not reached at $\alpha + \beta = 1$. In Fig. 5 we observe the appearance of three pronounced maxima of θ_J on shifted positions, approximately at $\alpha + \beta = 1.04$, 1.12 and 1.10, for $\alpha = 0.7$, 0.5 and 0.3, respectively. These maxima are not positioned at $\alpha + \beta = 1$ due to the uncertainty in the position of the particle within the cell. Actually, for $\beta \gtrsim 1 - \alpha$ excluded volume interaction with disks belonging to neighboring cells still substantially lowers the average number of adsorbed disks per-cell. As the parameter $\beta > 1 - \alpha$ is increased further to the critical value
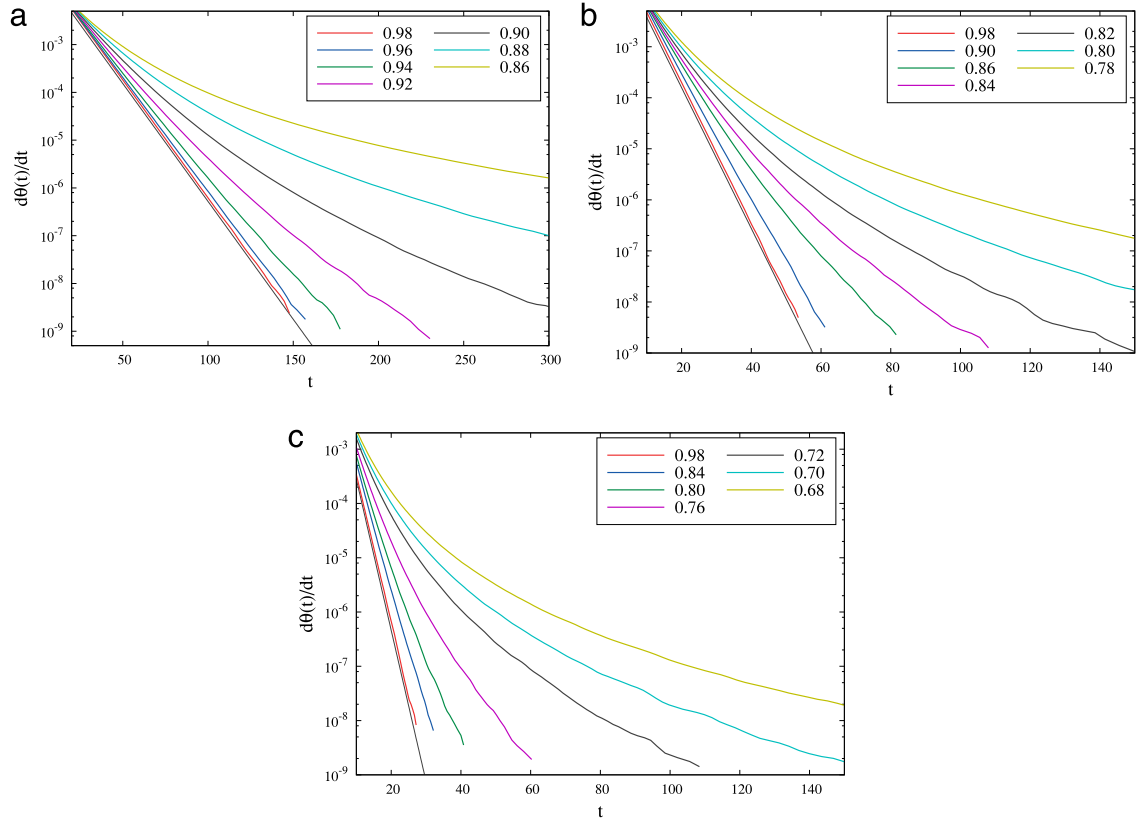
Fig. 4. Plots of the time derivative of coverage $d\theta/dt$ for the three values of cell size, $\alpha = 0.3$ (a), 0.5 (b), 0.7 (c). As indicated in the legend, the results are reported for values of the gap β above the corresponding critical values (Eq. (4)), $\beta_c = 0.85$ (a), 0.75 (b), 0.65 (c). Additionally, the slanted straight line is shown, indicating the exponential approach to the jamming limit (Eq. (2)), where $\sigma = 8.80$ (a), 3.15 (b), and 1.56 (c).
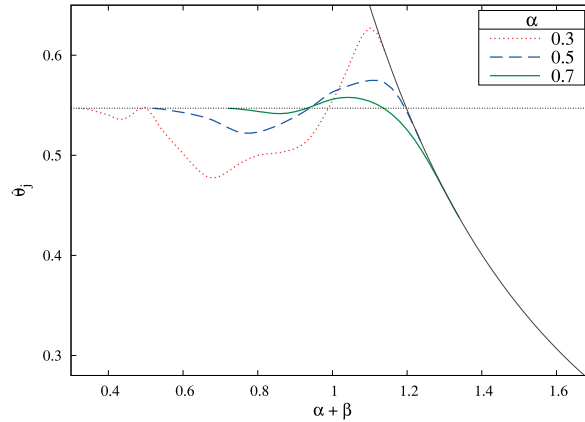

Fig. 5. Jamming coverage θ_J as a function of separation distance $\alpha + \beta$ (in units of the disk diameter d_0) for various values of the cell size α, as indicated in the legend. The solid black line indicates values of the jamming coverages θ_J^c calculated from Eq. (5).

β_c (Eq. (4)), the average cell population rises, and the jamming coverage θ_J increases until the appearance of large void space between the cells, when it falls to the value given by Eq. (5).

We also study the influence of varying α on the jamming coverage θ_J and on the late time kinetics of deposition process. We carried out a series of simulations at fixed $\alpha + \beta = 1.0$, 1.1, and varied cell size α. Numerical results regarding the jamming coverages θ_J for various α are shown in Fig. 6. For $\alpha + \beta = 1.1$, the criteria (3) cannot be satisfied if $\alpha < 0.2$. Therefore, for $\alpha < 0.2$ each cell host exactly one particle in the jamming state so that jamming coverage has the constant value $\theta_J = 0.6491$ given by Eq. (5). As $\alpha > 0.2$ increases, the cell–cell exclusion leads to a further reduction of the average
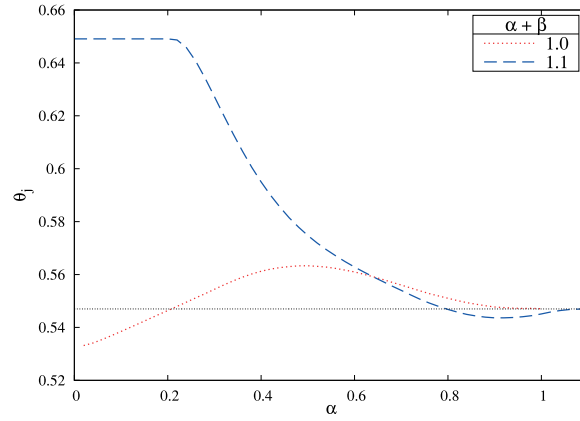
Fig. 6. Jamming coverage θ_J as a function of cell size α (in units of the disk diameter d_0) for two values of separation distance $\alpha + \beta$, as indicated in the legend.
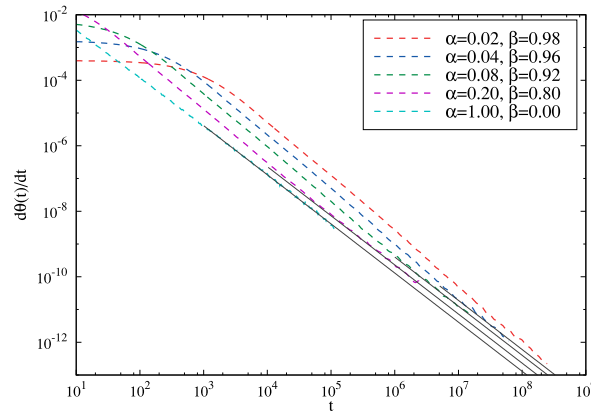
Fig. 7. Test for the presence of the algebraic law (1) in the approach of the coverage $\theta(t)$ to the jamming limit θ_J for different values of parameters α and β that satisfy the condition $\alpha + \beta = 1$ (see legend). Straight line sections of the curves show where the law holds. The solid straight lines have the slope $-3/2$ and are guides for the eye.

cell population, thereby making the jamming coverage lower. However, in the case of $\alpha + \beta = 1$ the jamming coverage $\theta_J(\alpha)$ increases first and reaches the wide maximum at $\alpha \approx 0.5$, after that the curve $\theta_J(\alpha)$ is lowered to the jamming value for continuum substrate θ_J^{cont}. For $\alpha < 1 - \sqrt{2}/2 \approx 0.3$, a cell can only be blocked by disks deposited at the nearest lateral neighbor cells. In that case, for more cell–cell exclusion effects, it is needed a smaller cell size. But, when cells are larger than $1 - \sqrt{2}/2$, a cell can also be blocked by disks deposited at the nearest diagonal neighbor cells, which enhances the cell–cell excluded volume interaction. These two opposite effects that exist when cells increase lead to the formation of the maximum of $\theta_J(\alpha)$ around $\alpha \approx 0.5$. Furthermore, when $\alpha + \beta = 1$ there is discontinuity of the function $\theta_J(\alpha)$ at $\alpha = 0$, since $\theta_J(0) = \pi/4 \approx 0.7854$, but $\lim_{\alpha \to 0^+} \theta_J(\alpha) < \theta_J^{cont} \approx 0.5472$.

3.3. Effects of varying α on the long-time adsorption kinetics

It is interesting that in the case when $\alpha + \beta = 1$, the approach to the jamming coverage θ_J is always algebraic, regardless of the size α of the landing cells. As can be seen from the Fig. 7, we find that for $\alpha \geqslant 0.02$ the coverage θ reaches a power-law time-behavior (1) within the length of the simulation. If a cell size α decreases, the value $\beta + \alpha/2$ increases and gets closer to unity when the condition (3) ceases to be valid. For very small cells ($\alpha \gtrsim 0$), the coverage growth is slowed down by the creation of smaller fraction of the layer that is available for the insertion of a new particle. Consequently, when cell size α decreases the onset of long-time power-law behavior (1) shifts to later times (Fig. 7). Generally, this effect occurs when the geometry of the pattern is close to the condition (4). In this case, it was necessary to increase the size of the substrate (typically 1024 × 1024 cells) in order to gain a convincing confirmation of power-law approach of the coverage fraction $\theta(t)$ to the jamming limit θ_J at the very late times of the deposition process.

When $\alpha + \beta = 1.1$, although there is no change of jamming coverage θ_J for $\alpha < 0.2$ (Fig. 6), changes in the dynamics of deposition are obvious (see Fig. 8). The criteria (3) is satisfied for $\alpha > 0.2$ and then the approach to the jamming limit is
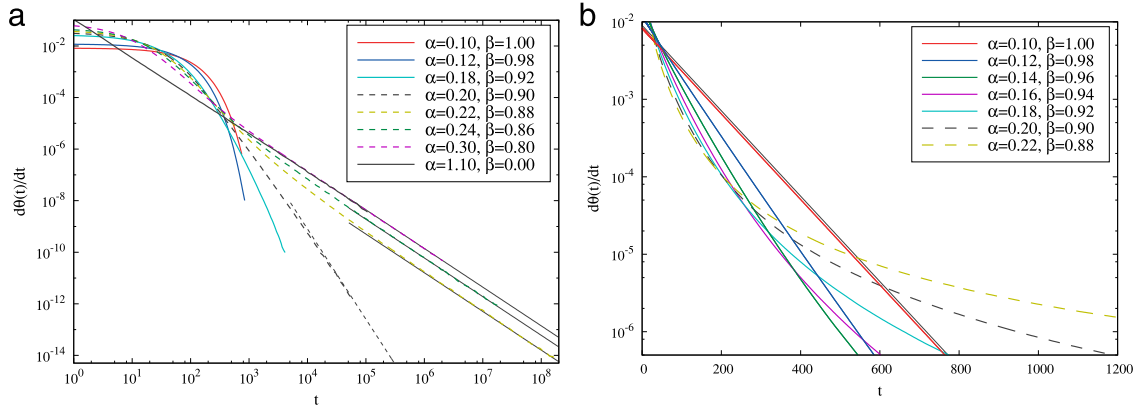
Fig. 8. Plots of the time derivative of coverage $d\theta/dt$ for different values of parameters α and β that satisfy the condition $\alpha + \beta = 1.1$ (see legends): (a) results are shown on a double logarithmic scale. Solid straight lines have the slope $-3/2$ and are guides for the eye. Dashed straight line has slope $-5/2$ indicating the late time RSA behavior of the system for the critical value of parameter β, $\beta_c = 0.20$ (see Eq. (4)); (b) results for $\alpha \leqslant 0.22$ are shown on a semilogarithmic scale. Slanted straight line is shown, indicating the exponential approach to the jamming limit (Eq. (2)), where $\sigma = 78.8$.

consistent with the power law behavior given by Eq. (1). As seen from Fig. 8(a), at the late times of the deposition process the plots of $d\theta/dt$ *vs.* t are linear on a double logarithmic scale with the slope of $-3/2$ for all $\alpha > 0.2$. However, the slope of $d\theta/dt$ abruptly changes to $\approx -5/2$ when the cell size α reaches the critical value of $\alpha = 0.2$ (see Eq. (4)). By reducing the size of cells below the critical value $\alpha = 0.2$, algebraic approach disappears. Under conditions when the cell size α decreases towards noninteracting condition $(\alpha \to 0.10^+, \beta \to 1.0^-)$, asymptotic approach of the coverage fraction $\theta(t)$ to its jamming limit θ_J becomes closer to the exponential law (2) (see Fig. 8(b)).

3.4. Spatial distribution of particles inside the cell

In order to gain additional insight into the late time kinetics of deposition process onto a nonuniform substrate it is useful to analyze in particular the spatial distribution of particles inside the cells. In Figs. 9, 10, and 11 we show the spatial distribution of particles inside the cell at the jammed state, for $\alpha = 0.3, 0.5$ and 0.7, respectively, and for the twelve different values of parameter $\beta \in [0.02\ 0.98]$. To calculate these probability distributions, we divided cell space in mesh with 40×40 bins and counted the number of particles falling into bins. The data are averaged over 100 independent runs for each of the investigated substrate patterns with 256×256 landing cells. Spatial distribution of particles shown in Figs. 9–11 are accompanied by corresponding radial distribution functions $g(r)$ (or pair-correlation functions) defined as

$$g(r) = \frac{S}{N^2} \left\langle \sum_{i=1}^{N} \sum_{j=1}^{N} \delta\left[\vec{r} - (\vec{r}_j - \vec{r}_i)\right] \right\rangle, \tag{6}$$

where $\vec{r}$ is the position vector of a point over the adsorption plane (measured from the center of an adsorbed particle), δ is the Dirac delta function, $\vec{r}_i$ and $\vec{r}_j$ are the position vectors of the particles i and j, respectively, and angle brackets mean the ensemble average. Here, S is the surface area, and N is the total number of particles adsorbed over this area. Radial distribution $g(r)$ gives information about the long-range interparticle correlations and their organization [13,49]. This function can be interpreted as an averaged probability of finding a particle at the distance r from another particle, with the center located at $r = 0$. For sake of convenience, the distance r is usually normalized by using the particle radius $d_0/2$ as a scaling variable. In the absence of external forces, when the system can be considered as isotropic, the vector $\vec{r}$ can be replaced with the radial coordinate r and the pair correlation function may be calculated more directly by converting Eq. (6) to the form

$$g(r) = \frac{S}{N} \frac{\overline{N}_a(r)}{2\pi r \Delta r}, \tag{7}$$

where $\overline{N}_a$ is the averaged number of particles within the annulus of the radius r and the thickness Δr.

To discuss the effect of the parameter β on the spatial distribution of particles inside the cell at the jammed state, let us first consider the fixed value $\alpha = 0.3$, with varying $\beta = 0.02 - 0.98$, as shown in Fig. 9. In the case of ICCA regime, the temporal evolution of the coverage $\theta(t)$ towards its jamming state value θ_J is a two-stage process. At very early times of the process, when the coverage fraction is small, the coverage grows rapidly in time. Particles adsorbed during this stage are homogeneously distributed in the cells. At late enough time, when the coverage fraction is sufficient to make the geometry of the unoccupied substrate complex, the growth of the coverage fraction $\theta(t)$ requires the filling of holes that are large enough for the insertion of an additional particle. Consequently, the structure of the spatial distribution of particles inside the cell
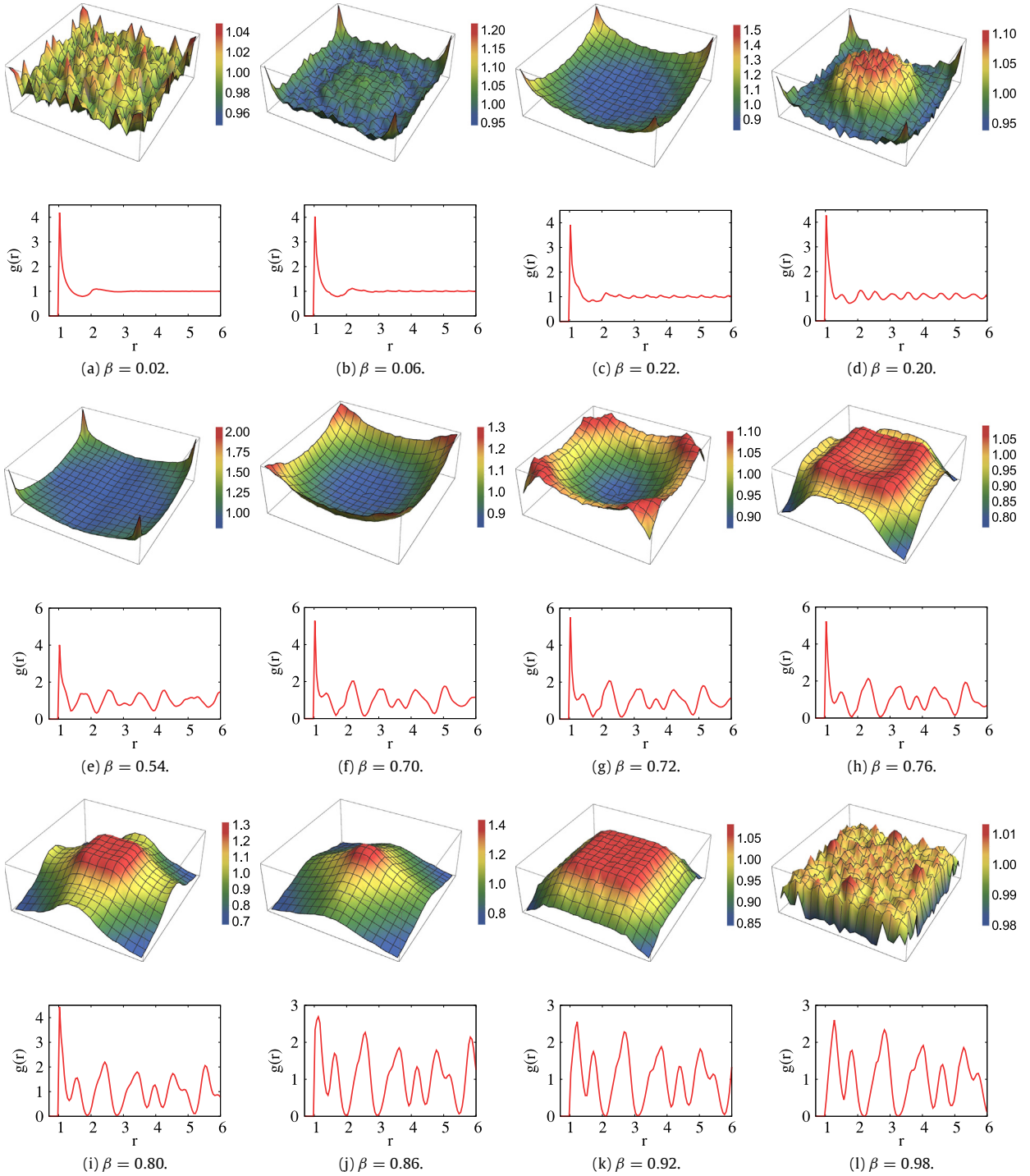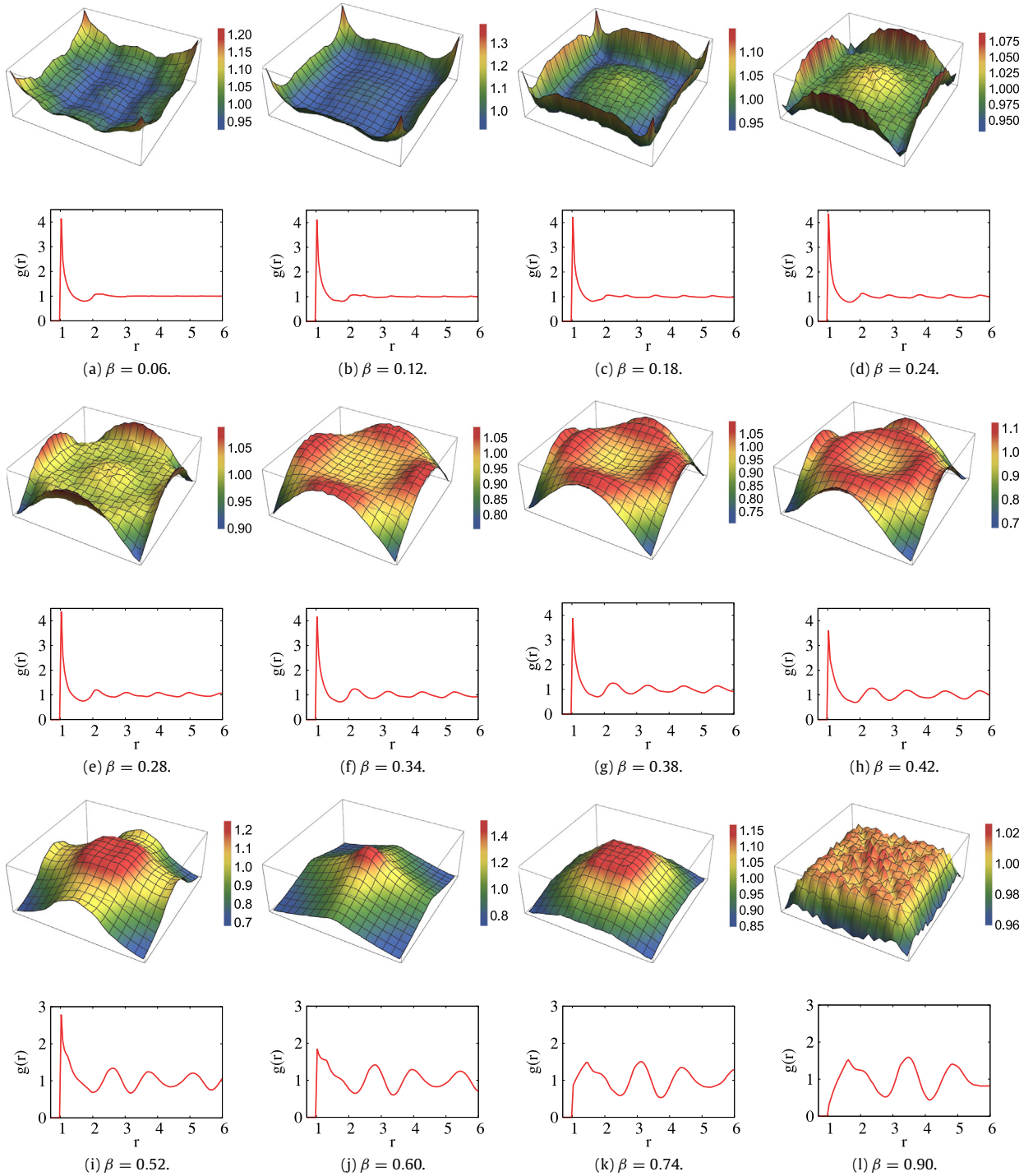
Fig. 9. Spatial distribution of particles inside the cell and radial distribution function $g(r)$ at the jammed state, for the fixed value of cell size $\alpha = 0.3$ and different values of parameter β.

is determined by the late stage of the deposition process. For $\beta \leqslant 0.02$, particles are distributed uniformly throughout the whole substrate and the shape of radial distribution $g(r)$ is the same as in the case of RSA of disks on a continuous substrate. Since the cell–cell excluded volume interaction is changing with β, the spatial distribution of particles inside the cell reveals various preferential regions. From the probability distribution plots in Fig. 9, we can identify various regions such as corners
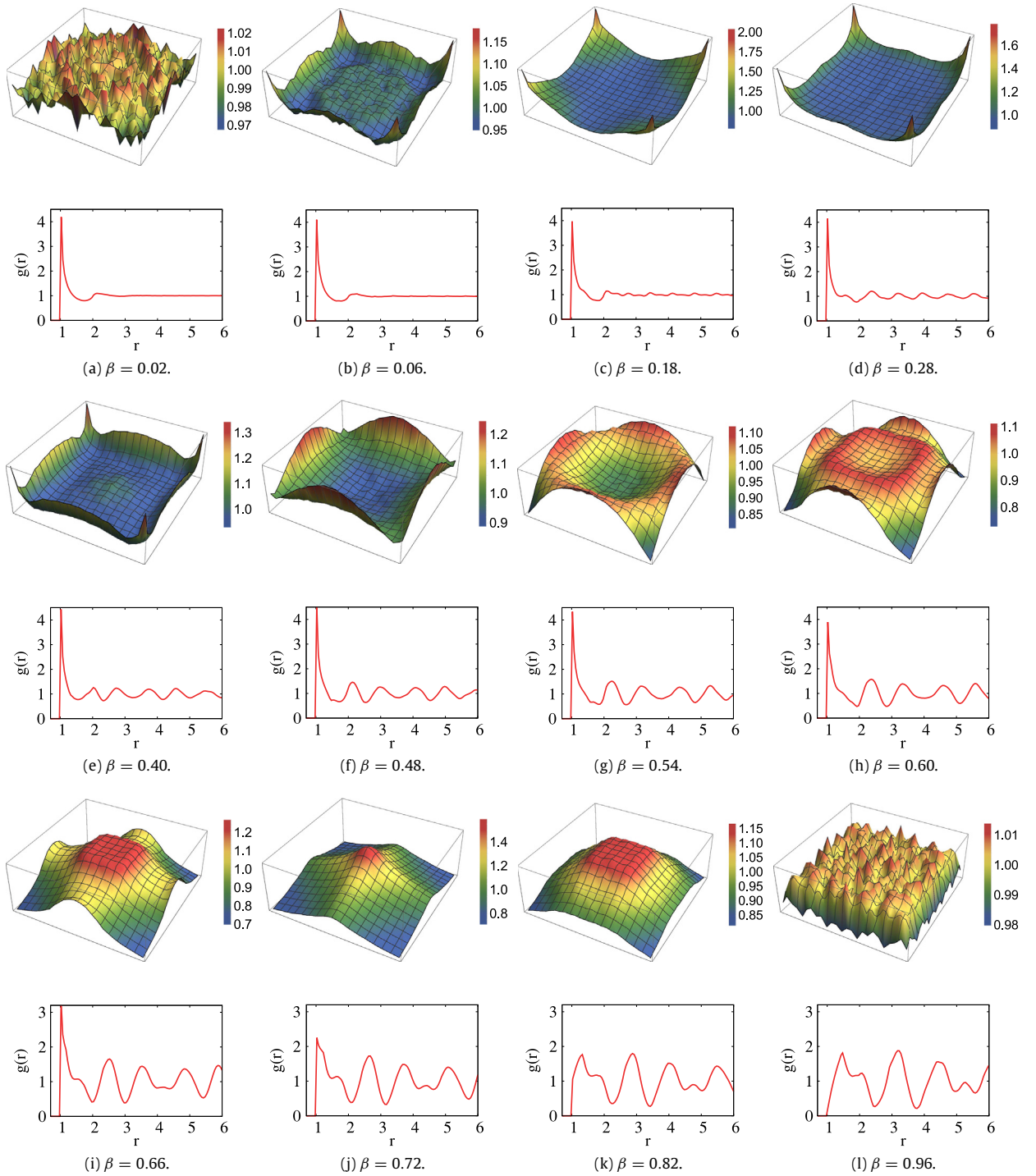
Fig. 10. Spatial distribution of particles inside the cell and radial distribution function $g(r)$ at the jammed state, for the fixed value of cell size $\alpha = 0.5$ and different values of parameter β.

(f), sides (g), interior ring (h), central square (i), central peak (j), etc., that are predominantly populated with particles. For β below the critical value β_c (Eq. (4)) particles adsorb preferentially at the cell edges. Approaching the critical value of $\beta_c = 0.85$ ($\alpha = 0.30$), the probability of deposition in the center of cell increases. Close to the critical value, we observe the appearance of pronounced peak of probability distribution in the center of the cell. In addition, as parameter β is increased,

Fig. 11. Spatial distribution of particles inside the cell and radial distribution function $g(r)$ at the jammed state, for the fixed value of cell size $\alpha = 0.7$ and different values of parameter β.

one observes that the radial distribution functions $g(r)$ becomes more detailed with peaks becoming sharper. There is also peak splitting, related to a weaker excluded volume interaction between particles deposited into different cells. For the large $\beta = 0.98$, since adsorption on an empty cell is weakly constrained by particles previously adsorbed on a neighboring one, adsorption can occur, with almost equal probability all over the cell (Fig. 9(l)). The radial distribution function now shows a

series of well developed peaks which correspond to the various cell-defined distances in the square lattice matrix. Finally, in the NICCA regime ($\beta > 1$), the adsorption inside cells is entirely uniform and the shape of the radial distribution function $g(r)$ is no longer changing (not shown here).

Numerical simulations for the other cell sizes, $\alpha = 0.5, \ 0.7$, produce qualitatively similar results for the spatial distribution of particles inside the cell leading to qualitatively same phenomenology (see Figs. 10 and 11). However, increasing the value of α in the NICCA-SPCA regime increases the uncertainty in the position of the particle within the cell, i.e., it leads to peak broadening of the radial distribution function $g(r)$.

4. Concluding remarks

We have investigated numerically RSA of disk-shaped particles on nonuniform planar substrates, with focus on the kinetics of deposition process in the interacting cell–cell adsorption (ICCA) regime. We have considered as a pattern the equal-size cells with square shape, positioned in a square-lattice matrix. An efficient numerical algorithm was implemented to simulate the disk deposition in the case of single particle per-cell adsorption (SPCA).

It was demonstrated that the two geometrical parameters, the cell size α and the cell–cell separation β, have a striking influence on the kinetic properties of a deposition process, as well as on the in-cell particle population. By studying the temporal evolution of the first derivative of coverage $\theta(t)$ we have found that the asymptotic approach of the coverage fraction $\theta(t)$ to its jamming limit θ_J is algebraic if the parameters α and β satisfy the simple condition (3). If the relation (3) is valid, particles adsorbed on neighboring cells can block adsorption inside the central cell, so that there is no minimum finite area available for adsorption. A vanishing-small area can be created with non-zero probability and power law (1) holds in the late stage of the deposition process.

If the geometry of the pattern does not satisfy the criteria (3), the approach of the coverage fraction $\theta(t)$ to the jamming limit is not consistent with the power law behavior. The existence of the minimum finite area where the center of a disk can land without overlapping a previously adsorbed particle is a sufficient condition for deviation from the algebraic asymptotic approach (1). When the geometry of the pattern approaches towards noninteracting condition ($\beta \to 1.0^-$), the asymptotic approach of the coverage fraction $\theta(t)$ to its jamming limit θ_J becomes closer to the exponential law (2). It must be stressed that the appearance of even a slight cell–cell excluded volume interaction violates the exponential asymptotic approach. Consequently, changing the pattern in our numerical model allows to interpolate the deposition kinetics between the continuum limit and the lattice-like behavior.

To examine the short scale structure in the jammed-state coverings, we evaluated the spatial distribution of particles inside the cell and radial distribution function $g(r)$. Interesting, non-trivial spatial distributions are observed, with local order resulting not only from the constraint of the pattern, but also due to steric effects that make certain insertions of particles impossible owing to an effective high local density. Close to the critical values of parameters α and β determined with Eq. (4), we observe the appearance of the pronounced peak of probability distribution in the center of the cell. Hence, by tuning the pattern parameters on the critical values (Eq. (4)), it is possible to obtain jammed-state covering with high ordered structure.

Acknowledgments

References

[1] Irving R. Epstein, Kinetics of large-ligand binding to one-dimensional lattices: theory of irreversible binding, Biopolymers 18 (1979) 765–788.
[2] Paul R. Van Tassel, Pascal Viot, Gilles Tarjus, A kinetic model of partially reversible protein adsorption, J. Chem. Phys. 106 (1997) 761–770.
[3] J. Feder, Random sequential adsorption, J. Theoret. Biol. 87 (1980) 237.
[4] S. Ravichandran, J. Talbot, Mobility of adsorbed proteins: a brownian dynamics study, Biophys. J. 78 (2000) 110–120.
[5] Vladimir Privman, Recent theoretical results for nonequilibrium deposition of submicron particles, J. Adhes. 74 (2000) 421–440.
[6] J. Alexander Liddle, Yi Cui, Paul Alivisatos, Lithographically directed self-assembly of nanostructures, J. Vac. Sci. Technol., B: Microelectron. Nanometer Struct. Process., Meas., Phenom. 22 (2004) 3409–3414.
[7] Arsen V. Subashiev, Serge Luryi, Random sequential adsorption of shrinking or expanding particles, Phys. Rev. E 75 (2007) 011123.
[8] Oleksandr Gromenko, Vladimir Privman, Random sequential adsorption of objects of decreasing size, Phys. Rev. E 79 (2009) 011104.
[9] Ranjan D. Deshmukh, Gavin A. Buxton, Nigel Clarke, Russell J. Composto, Nanoscale block copolymer templates decorated by nanoparticle arrays, Macromolecules 40 (2007) 6316–6324.
[10] J.W. Evans, D.R. Burgess, Irreversible reaction on a polymer chain with range two cooperative effects, J. Chem. Phys. 79 (1983) 5023–5028.
[11] C.S. Dias, N.A.M. Araújo, A. Cadilhe, Analytical and numerical study of particles with binary adsorption, Phys. Rev. E 85 (2012) 041120.
[12] Oleksandr Gromenko, Vladimir Privman, M.L. Glasser, Random sequential adsorption model of damage and crack accumulation: exact one-dimensional results, J. Comput. Theor. Nanosci. 5 (2008) 2119–2123.
[13] J.W. Evans, Random and cooperative sequential adsorption, Rev. Modern Phys. 65 (1993) 1281–1329.
[14] V. Privman (Ed.), Nonequilibrium Statistical Mechanics in One Dimension, Cambridge University Press, Cambridge, UK, 1997 (a collection of review articles).
[15] V. Privman, Colloids Surf. A 165 (2000) 1 (a collection of review articles).

[16] P. Parisse, D. Luciani, A. D'Angelo, S. Santucci, P. Zuppella, P. Tucceri, A. Reale, L. Ottaviano, Patterning at the nanoscale: atomic force microscopy and extreme ultraviolet interference lithography, Mater. Sci. Eng. B 165 (2009) 227–230.

[17] T. Kraus, L. Malaquin, H. Schmid, W. Riess, N.D. Spencer, H. Wolf, Nanoparticle printing with single-particle resolution, Nature Nanotechnol. 2 (2007) 570–576.

[18] R.J. Kershner, L.D. Bozano, C.M. Micheel, A.M. Hung, A.R. Fornof, J.N. Cha, C.T. Rettner, M. Bersani, J. Frommer, P.W.K. Rothemund, G.M. Wallraff, Placement and orientation of individual dna shapes on lithographically patterned surfaces, Nature Nanotechnol. 4 (2009) 557–561.

[19] A. delCampo, C. Greiner, I. Àlvarez, E. Arzt, Patterned surfaces with pillars with controlled 3d tip geometry mimicking bioattachment devices, Adv. Mater. 19 (2007) 1973–1977.

[20] Z. Adamczyk (Ed.), Particles At Interfaces: Interactions, Deposition, Structure, in: Interface Science and Technology, vol. 9, Elsevier, 2006.

[21] X. Jin, N.H.L. Wang, G. Tarjus, J. Talbot, Irreversible adsorption on non-uniform surfaces: the random site model, J. Chem. Phys. 97 (1993) 4256.

[22] X. Jin, J. Talbot, N.H.L. Wang, Analysis of steric hindrance effects on adsorption kinetics and equilibria, AIChE J. 40 (1994) 1685.

[23] C. Oleyar, J. Talbot, Reversible adsorption on random site surface, Physica A 376 (2007) 27–37.

[24] Z. Adamczyk, P. Weronski, E. Musial, Irreversible adsorption of hard spheres at random site (heterogeneous) surfaces, J. Chem. Phys. 116 (2002) 4665.

[25] Z. Adamczyk, B. Siwek, P. Weronski, E. Musial, Irreversible adsorption of colloid particles at heterogeneous surfaces, Appl. Surf. Sci. 196 (2002) 250.

[26] Zbigniew Adamczyk, Katarzyna Jaszczt, Aneta Michna, Barbara Siwek, Lilianna Szyk-Warszyska, Maria Zembala, Irreversible adsorption of particles on heterogeneous surfaces, Adv. Colloid Interface Sci. 118 (2005) 25–42.

[27] A. Cadilhe, N.A.M. Araújo, V. Privman, Random sequential adsorption: from continuum to lattice and pre-patterned substrates, J. Phys.: Condens. Matter 19 (2007) 065124.

[28] N.A.M. Araújo, A. Cadilhe, Vladimir Privman, Morphology of fine-particle monolayers deposited on nanopatterned substrates, Phys. Rev. E 77 (2008) 031603.

[29] J.F. Marques, A.B. Lima, N.A.M. Araújo, A. Cadilhe, Effect of particle polydispersity on the irreversible adsorption of fine particles on patterned substrates, Phys. Rev. E 85 (2012) 061122.

[30] N. Araujo, Nonequilibrium Thin-Film Growth: Kinetics of Deposition and Post Evolution Relaxation, LAP LAMBERT Academic Publishing, 2010.

[31] D. Stojiljković, J.R. Šćepanović, S.B. Vrhovac, N.M. Švrakić, Structural properties of particle deposits at heterogeneous surfaces, J. Stat. Mech. Theory Exp. 2015 (2015) P06032.

[32] P. Philippe, D. Bideau, Numerical model for granular compaction under vertical tapping, Phys. Rev. E 63 (2001) 051304.

[33] P. Richard, P. Philippe, F. Barbe, S. Bourles, X. Thibault, D. Bideau, Analysis by x-ray microtomography of a granular packing undergoing compaction, Phys. Rev. E 68 (2003) 020301(R).

[34] T. Aste, Variations around disordered close packing, J. Phys.: Condens. Matter 17 (2005) S2361–S2390.

[35] T. Aste, Volume fluctuations and geometrical constraints in granular packs, Phys. Rev. Lett. 96 (2006) 018002.

[36] D. Arsenović, S.B. Vrhovac, Z.M. Jakšić, Lj. Budinski-Petković, A. Belić, Simulation study of granular compaction dynamics under vertical tapping, Phys. Rev. E 74 (2006) 061302.

[37] R. Swendsen, Dynamics of random sequential adsorption, Phys. Rev. A 24 (1981) 504–508.

[38] Y. Pomeau, Some asymptotic estimates in the random parking problem, J. Phys. A: Math. Gen. 13 (1980) L193.

[39] B. Bonnier, Random sequential adsorption of binary mixtures on a line, Phys. Rev. E 64 (2001) 066111.

[40] D.J. Burridge, Y. Mao, Recursive approach to random sequential adsorption, Phys. Rev. E 69 (2004) 037102.

[41] EinarL Hinrichsen, Jens Feder, Torstein Jøssang, Geometry of random sequential adsorption, J. Stat. Phys. 44 (1986) 793–827.

[42] M.C. Bartelt, V. Privman, Kinetics of irreversible multilayer adsorption: one-dimensional models, J. Chem. Phys. 93 (1990) 6820.

[43] S.S. Manna, N.M. Švrakić, Random sequential adsorption: line segments on the square lattice, J. Phys. A: Math. Gen. 24 (1991) L671–L676.

[44] Lj. Budinski-Petković, U. Kozmidis-Luburić, Random sequential adsorption on a triangular lattice, Phys. Rev. E 56 (1997) 6904.

[45] Lj. Budinski-Petković, S.B. Vrhovac, I. Lončarević, Random sequential adsorption of polydisperse mixtures on discrete substrates, Phys. Rev. E 78 (2008) 061603.

[46] Vladimir Privman, Han Yan, Random sequential adsorption on imprecise lattice, J. Chem. Phys. 144 (2016) 244704.

[47] Einar L. Hinrichsen, Jens Feder, Torstein Jøssang, Random packing of disks in two dimensions, Phys. Rev. A 41 (1990) 4199–4209.

[48] P.G. Szabó, M.Cs. Markót, T. Csendes, E. Specht, L.G. Casado, I. García, New approaches to circle packing in a square (with program codes), in: Optimization and Its Applications, Vol. 6, Springer Science + Business Media, LLC, New York, USA, 2007.

[49] Thomas M. Truskett, Salvatore Torquato, Srikanth Sastry, Pablo G. Debenedetti, Frank H. Stillinger, Structural precursor to freezing in the hard-disk and hard-sphere systems, Phys. Rev. E 58 (1998) 3083–3088.